Fibril Size-Dependent Control of Polar Ordering in Type I Collagen Membranes

Fengyuan Zhang and Brian J. Rodriguez
School of Physics & Conway Institute of Biomolecular and Biomedical Research
University College Dublin,
Belfield, Dublin 4, Ireland

Steven Sawamura and Michael V. Paukshto
Fibralign Corporation
32930 Alvarado-Niles Rd., Suite 350
Union City, California 94587, United States

The most abundant protein in the human body, collagen, is widely used in tissue culture and engineering applications, spanning from substrate functionalization to fibrillar architectures and three-dimensional constructs. Collagen piezoelectricity provides an opportunity to exploit electromechanical coupling in these applications, wherein an applied mechanical stress generates charge, which might influence ion screening, protein absorption, and cell response. In type I collagen, the polarization direction follows the fibril orientation. Thus, control of fibril orientation and size in a collagen film or membrane may provide control of the polarization, enabling the creation of regions of uniform polarization direction. Here, aligned substrate-supported type I collagen membranes having fibril sizes from ~100–500 nm are deposited using different osmotic concentrations (90, 190, and 290 mOsm/kg, from low to high ionic strength) to investigate the correlation between fibril size and piezoelectric properties. Lateral piezoresponse force microscopy is used to show that regions of uniform polarization orientation, as determined through 2D correlation analysis, decrease with increasing fibril size.

Keywords: piezoelectric films, piezoelectricity, polarization, biomedical materials

1 INTRODUCTION

In the past few decades, piezoelectricity has been investigated in type I collagenous materials such as teeth, bone, tendon, cornea, and fish scales [1–5] building on the pioneering work of Fukada and co-authors in the preceding decades [6, 7]. Piezoelectricity has also been found on other organic materials such as diphenylalanine peptide-based structures [8, 9]. Compared to inorganic piezoelectric materials such as lead zirconate titanate, commonly used in sensing and actuating applications, organic piezoelectrics are more environmentally-friendly [10]. Moreover, organic piezoelectrics can be used in a range of biomedical applications [11], *e.g.*, in tissue culture and engineering, as well as in energy harvesting applications, as demonstrated using viruses (M13 bacteriophages), collagen, and peptide nanotubes (PNTs) [1, 12-14]. For example, Ghosh and Mandal reported a collagen-based fish scale nanogenerator with a power output density of 1.14 $\mu W/cm^2$ under a compressive stress of 0.17 MPa [1]. Recently, Lee *et al* reported that the polarization direction distribution of the PNTs (along the long axis of the PNT) has a critical effect on the energy harvesting; polarization-aligned structures yielded ~10 times the voltage output of randomly-oriented structures [14].

Similar to PNTs, the polarization direction of a collagen fibril, defined by the amine to carboxyl dipole of the collagen molecule building blocks of the fibril, is also along its long axis [8, 15], and attempts to control and align the polarization direction of collagen fibrils may prove beneficial in energy harvesting and tissue engineering applications. For example, cell motion, proliferation, and differentiation have been reported to be sensitive to an applied external electric field [16], and cell function has been reported to be affected by local flexoelectrically-

generated fields in bone [17]. A piezoelectric collagen surface with tailored polarization domain size may be able to affect cell behavior through the generation of mechanically-induced charge.

Prior work reported that the polarization directions of collagen fibrils, as determined by piezoresponse force microscopy (PFM) or second harmonic generation, within native and engineered tissues tend to be arranged randomly, even for tissues containing highly ordered, aligned fibrils (often in an antiparallel configuration) [4, 15, 18–20]. As a result, within a cross sectional area of a tendon with aligned collagen fibrils, the net polarization would be ~zero [3]. While no prior work has shown uniform polarity in a collagenous tissue, a previous study reported that regions of uniform PFM phase larger than the topographic features were observed in type I collagen films [2], and aligned collagen membranes have been prepared from a type I collagen nematic liquid crystal phase on glass slides under shear flow [21] with regions of ~20 fibrils having the same polar direction [19]. Here, we investigate the effect of osmolality (concentration expressed as total number of solutes per kg of water) on the fibril width and uniform-polarity domain size in aligned type I collagen membranes. We prepared membranes having fibril sizes in the range from ~100–500 nm and use lateral PFM (LPFM) to characterize the piezoelectric properties of membranes, finding that as the fibril size decreases, the area of uniform polarity increases.

2 EXPERIMENTAL

2.1 SAMPLE PREPARATION

The aligned collagen membranes (Fibralign) were produced from medical grade monomeric porcine type I atelocollagen in a nematic liquid crystal state (~60 mg/ml) with different osmolalities (90, 190, and 290 mOsm/kg, from low to high ionic strength) under controlled shear flow on glass slides (0.8 cm × 1.5 cm), with fibrils forming during evaporation of the liquid crystal [21]. One 90 mOsm/kg sample, later referred to as having ultra-small fibrils, was prepared at a lower than ambient relative humidity (<30%).

2.2 SAMPLE CHARACTERIZATION

Topography and piezoelectric properties of the collagen membranes were measured using atomic force microscopy (AFM; Cypher, Asylum Research). The nominal spring constant and resonant frequency of the conductive cantilevers (PPP-EFM, Nanosensors) used in all measurements were 2.5 N/m and 75 kHz, respectively. All samples were imaged with the long axis of the cantilever orthogonal to the overall alignment direction of the collagen. Contact-mode topography images were recorded simultaneously with lateral LPFM (also known as in-plane PFM) using a 30 nN loading force. A 15 kHz alternating current (AC) voltage of 60 V (peak-to-peak) applied to the conducting probe to excite surface deformations via the converse piezoelectric effect and monitor cantilever torsion. A voltage amplifier (F10A, FLC Electronics AB) was used to amplify the AC voltage from the lock-in amplifier (HF2LI, Zurich Instruments), which was also used to demodulate the LPFM amplitude (depends on piezoelectric response) and phase (depends on polar orientation) signals. Piezoelectric data were also recorded at specific locations while sweeping the AC voltage from 0 to 60 V, wherein the slope provides a measure of the effective shear piezoelectric coefficient, d_{15}. Calibration of the LPFM signal required determination of the lateral inverse optical lever sensitivity, which was calculated by multiplying the measured vertical inverse optical lever sensitivity (~50 pm/V with less than 1% variation before and after measurements) by the in-plane to out-of-plane amplification ratio, R, given by $R = 2L/3h$ [22] using typical values for L, the length of the cantilever, and h, the combined tip length and cantilever thickness.

2.3 AUTOCORRELATION ANALYSIS

LPFM images were assessed using 2D autocorrelation analysis. Firstly, autocorrelation images, $C(r_1, r_2)$, were obtained from LPFM phase images via Equation (1):

$$C(r_1, r_2) = \sum_{x,y} D(x, y)D(x + r_1, y + r_2) \quad (1)$$

where $D(x, y)$ is the value of the LPFM phase signal. Secondly, the autocorrelation function was averaged over all in-plane directions of the autocorrelated images and approximated by Equation (2):

$$< C(r) > = \sigma^2 \exp[-(r/< \xi >)^{2p}] \quad (2)$$

In Equation (2), r is the distance from the central peak in the autocorrelation images, $<\xi>$ is the average correlation radius, and the exponent p ($0 < p < 1$) is a measure of the roughness of the so-called polarization interface.

3 RESULTS AND DISCUSSION

Topographic images (30 µm × 30 µm) of the prepared collagen membranes are shown in Figures 1a–1d, corresponding to membranes prepared with 290, 190, and 90 mOsm/kg at ambient relative humidity, and 90 mOsm/kg at <30% relative humidity. The white arrow in Figure 1a indicates the predominant fibril alignment direction for all samples and all figures. The fibrils in the membranes have a woven appearance, with local deviations from the alignment direction, while maintaining an overall predominant alignment. The osmolality appears to control the fibril size, or at least the topographical features. The woven appearance of the fibrils evolves with reducing fibril size, leading to a ramen-like structure in Figure 1c and notable horizontal features in Figure 1d, reminiscent of tendon-like crimp features as noted previously by Denning *et al* [19]. The average size of the fibrils (or fibril bundles) was determined by analyzing orthogonal line profile cross sections of 20 apparent fibrils from each membrane shown in Figures 1a–1d to be 476 ± 115 nm, 308 ± 108 nm, 276 ± 86 nm, 123 ± 17 nm, respectively (determined using 10 µm × 10 µm and 5 µm × 5 µm images). For convenience, we will refer to the membranes as having large, medium, small, and ultra-small fibrils (Table 1). The standard deviation increases with fibril size, reflecting a larger size distribution for membranes with larger fibrils, consistent with the appearance (Figures 1a–1d) and roughness (determined from 30 µm × 30 µm images) of the membranes (Table 1). The root-mean-square roughness was determined to be 120, 113, 38, and 9 nm in Figures 1a–1d, respectively, highlighting the role of osmolality in controlling topographical features. Perhaps as expected, the results show that thinner fibrils are more likely to form a smoother membrane surface. The role of ionic strength and pH on collagen fibril formation in solution or on a substrate has been highlighted before; previously, Morozova *et al* reported that thinner collagen fibrils formed in collagen solutions of lower ionic strengths [23]. Interestingly, a similar trend is observed for collagen membranes formed from a nematic liquid crystal state.

Table 1. Osmolality, fibril size, roughness, and correlation radius.

Sample	Osmolality (mOsm/kg)	Fibril size (nm)	Roughness (nm)	Correlation radius (nm)
Large	290	476 ± 116	120	75 ± 16
Medium	190	308 ± 108	113	340 ± 12
Small	90	276 ± 86	38	384 ± 17
Ultra-small	90	123 ± 17	9	474 ± 7

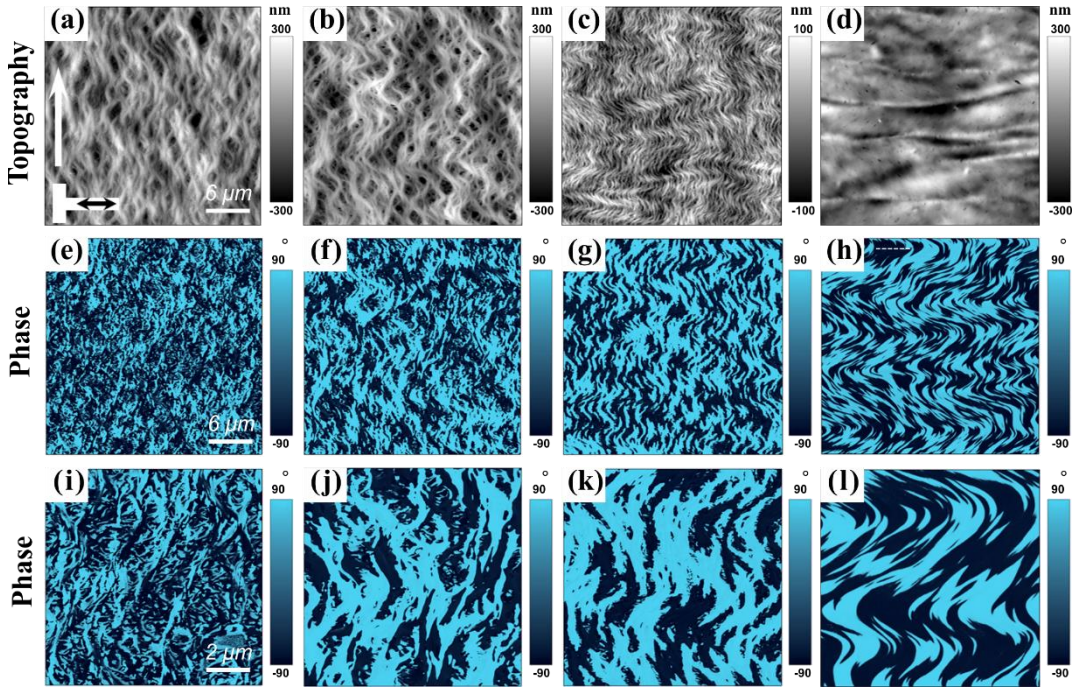

Figure 1. Topography and lateral piezoresponse force microscopy (LPFM) phase images. (a-d) Topography (30 μm × 30 μm) and corresponding (e-h) LPFM phase images of collagen membranes with (a, e) large, (b, f) medium, (c, g) small, and (d, h) ultra-small fibrils. (i-l) LPFM phase images from the central 10 μm × 10 μm area of (e-h). The white dashed line in (h) shows the largest domain width in these LPFM figures. The white arrow in (a) indicates the predominant fibril alignment direction, which is perpendicular to the cantilever (white). The black arrow in (a) indicates the scan direction of all images.

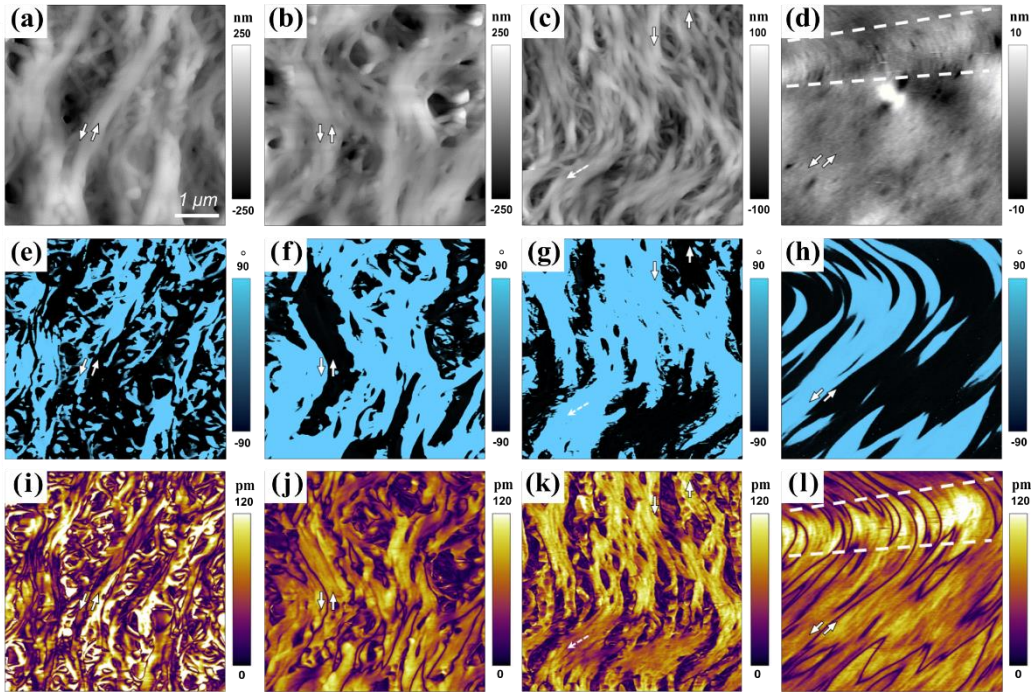

Figure 2. Topography and LPFM phase and amplitude images. (a-d) Topography and corresponding LPFM (e-h) phase and (i-l) amplitude images of collagen membranes with (a, e, i) large, (b, f, j) medium, (c, g, k) small (d, h, l), and ultra-small fibrils. The white solid arrows in each image point to two opposite polarization directions. The white dashed arrows in (c, g, k) show an example of fibrils that are not perpendicular to the cantilever. The dashed lines in (d, l) show a region where the LPFM amplitude reaches a maximum as the fibrils align perpendicular to the cantilever. Apparent fibril size was determined in (d) from regions where fibrils were visible, such as between the dashed lines. Scale bar in (a) applies to all images.

The LPFM phase images corresponding to the topography images in Figures 1a–1d are provided in Figures 1e–1h and show the polar orientation of the fibrils within each collagen membrane. There appears to be an influence of osmolality and thereby fibril size on the resultant domain pattern. Notably, the LPFM phase response appears to become more structured with decreasing osmolality. Since the polar direction is defined by the fibril and the fibrils are predominantly ordered orthogonal to the (horizontal) scan direction, the horizontal width of regions of uniform polarity is a good measure of the region of uniform polarity or domain size. It is worth mentioning that the maximum uniform polarity width in the membrane with ultra-small fibrils is 5.1 μm (shown as white dashed line in Figure 1h), which is more than 40 times the average fibril size. Unlike reports on other collagenous tissues where the polarity domain size tends to correspond to the fibril size, the LPFM phase image for the membrane with large fibrils (Figure 1e) appears to have domains smaller than the fibril size reported that do not correspond exactly with the apparent fibril alignment. To investigate this discrepancy, LPFM phase images of 10 μm × 10 μm and 5 μm × 5 μm regions were recorded (Figures 1i–1l and Figures 2a–2d, respectively). The average width of regions of uniform polarity (domains) was determined from 10 horizontal line profile cross sections of Figures 1i–1l to be 289 ± 194 nm, 476 ± 419 nm, 642 ± 497 nm, and 830 ± 764 nm, respectively. Figures 2a–2d show 5 μm × 5 μm topography images for the four membranes. Figure 2a reveals that the surface comprises fibril bundles and branching fibrils with a more complex topography than previously considered. Such a surface with intertwined fibrils could give rise to the LPFM phase images shown in Figures 1e, 1i, and 2e, resulting in domain sizes smaller than the apparent fibril size. Varying levels of topographic complexity persists in membranes with medium (Figure 2b) and small (Figure 2c) fibril sizes as well; however, with decreasing osmolality, the overlapping fibrils appear more likely to have the same polarization direction (Figures 2f and 2g), resulting in domains of uniform polarity that are larger than the fibril size. For the membrane with the ultra-small fibrils (Figure 2d), the fibrils form a more uniform layer and large polarity domains (Figure 2h). The topography and LPFM results are reproducible in different locations on each sample.

Even though the fibril and domain sizes are different for each collagen membrane, there are still similarities in their piezoresponse. For example, the fibrils which are perpendicular to the tip long axis have stronger piezoresponse than those at other angles. The dashed arrows in Figures 2c, 2g, and 2k show the apparent polarization direction of that area, which are not parallel to the alignment direction or orthogonal to the cantilever axis. Correspondingly, the LPFM amplitude in this region is lower, as expected and as previously reported by Denning *et al* [18]. Figure 2l also shows this behavior between the dashed lines, where the amplitude reaches a maximum as the fibril orientations become orthogonal to the long axis of the cantilever. Moreover, adjacent domains have opposite polarization directions (white arrows in Figures 2e–2h), having similar amplitude response and being separated by a minimum in the amplitude response.

To better evaluate the polarity domain size of the membranes, autocorrelation analysis was performed Figure 3). Such analysis has been previously used to investigate nanopolar structures in relaxor ferroelectrics [24]. Autocorrelation images (Figures 3a, 3b, 3d, and 3e) were obtained from LPFM phase images (Figures 1e–1h). The shape of the autocorrelation image provides information on the symmetry and regularity of the polarization distribution. In addition, the width of the central spot in the autocorrelation images shows the polarization correlation radius. The inset images in Figures 3a, 3b, 3d, and 3e show the center peak of the correlation images (2 μm × 2 μm area). Since the polarization direction coincides with the alignment direction, most domain sizes are larger in the vertical direction compared to the horizontal direction. This behavior is apparent in the autocorrelation images as well (oval shape of the center spot in Figures 3a, 3b, 3d, and 3e). The center spot becomes more symmetric for the membrane with the ultra-small fibril membrane because of the relatively larger domain width. The inset images also show that the center spot increases in size from Figure 3a to Figure 3b, which means the domain radius is increasing. The autocorrelation images are averaged over all in-plane directions and plotted in Figure 3c. After fitting each

curve in Figure 3c using Equation (2), the obtained autocorrelation radii were plotted in Figure 3f. We observed that the increased fibril size results in a decrease in the correlation radius from 474 to 75 nm (Table 1), a trend consistent with the analyzed averaged domain width.

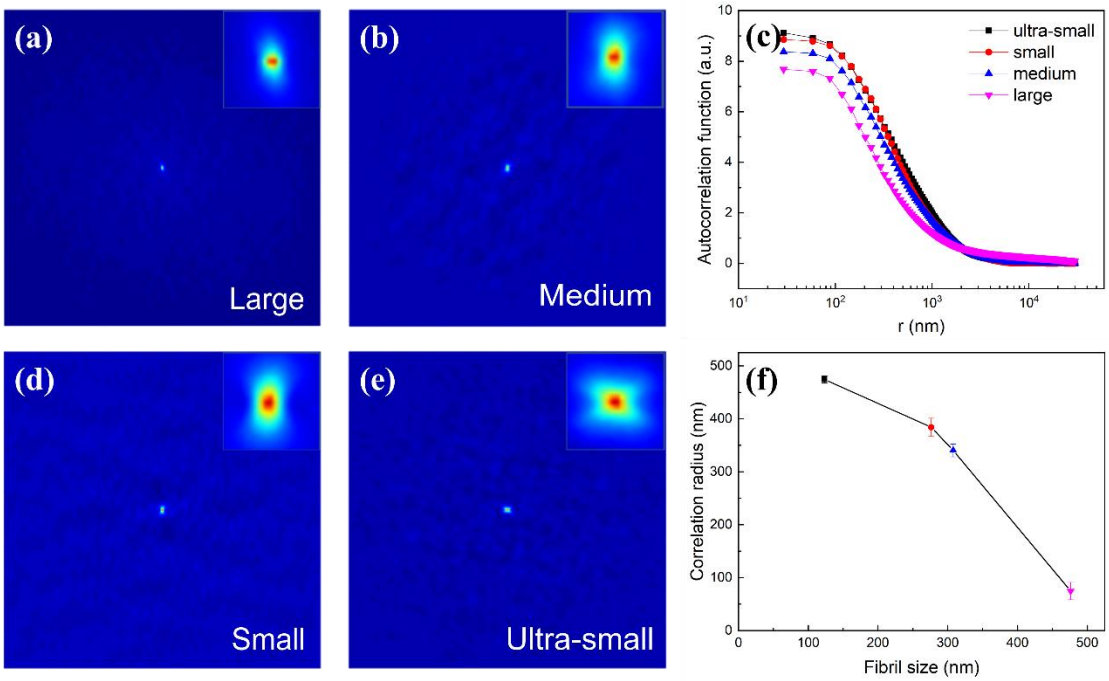

Figure 3. (a, b, d, e) Auto correlation images (60 µm × 60 µm) of LPFM phase images from Figures 1e–h. The insets show the center of each image (2 µm × 2 µm). (c) Distance dependence of the autocorrelation function, $C(r_1, r_2)$, averaged over all in-plane directions from the central maximum. (d) Fibril size dependence of the mean correlation radius of each collagen membrane (see Table 1).

The effective d_{15} coefficient of the membranes, determined from the slopes of the linear fits of the LPFM amplitude response versus applied AC voltage in the 6 to 30 V range, was 6.0 ± 1.0 pm/V. The d_{15} value reported here is similar to previous reports for type I collagen (6.21 ± 2.93 pm/V) [3] and higher than reported previously for type I collagen membranes [19]; however, those membranes were prepared with a different formulation and manufacturing process and the calibration procedure neglected to take into account the instrument-dependent vertical and lateral signal electronic gains [25]. Measurements performed using the same experimental set-up revealed an effective d_{15} of 8.2 ± 0.8 for type I collagen fibrils from murine tail tendon. These values give an indication of the relative shear piezoelectricity of the samples, noting that the calibration procedure used provides an estimate of the lateral inverse optical lever sensitivity rather than a direct measurement of it. As collagen has been demonstrated in energy harvesting applications [1], the collagen membranes reported here, that can be deposited on different substrates [21] with, to an extent, tunable fibril and polar domain size, may be suitable energy harvesting materials.

4 CONCLUSIONS

Aligned type I collagen membranes, prepared with average fibril sizes of 123 ± 17 nm, 276 ± 86 nm, 308 ± 108 nm, and 476 ± 116 nm were found by lateral piezoresponse force microscopy and 2D correlation analysis to have distinct characteristic domain sizes of uniform polarization that increased with decreasing fibril size. The ability to control the size of the regions with uniform polarization may have implications for tissue engineering and energy harvesting applications.

ACKNOWLEDGMENT

This research was funded by the European Union's Horizon 2020 research and innovation program under Marie Skłodowska-Curie grant agreement number 644175. This publication has emanated from research supported in part by the China Scholarship Council. B. J. R. acknowledges Sergei Kalinin for insightful discussions.

REFERENCES

[1] S. K. Ghosh and D. Mandal, "High-performance bio-piezoelectric nanogenerator made with fish scale," Appl. Phys. Lett., vol. 109, no. 10, pp. 232–236, 2016.
[2] B. J. Rodriguez *et al*, "Electromechanical imaging of biomaterials by scanning probe microscopy," J. Struct. Biol., vol. 153, no. 2, pp. 151–159, 2006.
[3] D. Denning *et al*, "Piezoelectric tensor of collagen fibrils determined at the nanoscale," ACS Biomater. Sci. Eng., vol. 3, no. 6, pp. 929–935, 2017.
[4] D. Denning *et al,* "Visualizing molecular polar order in tissues via electromechanical coupling," J. Struct. Biol., vol. 180, no. 3, pp. 409–419, 2012.
[5] M. Minary-Jolandan and M. F. Yu, "Uncovering nanoscale electromechanical heterogeneity in the subfibrillar structure of collagen fibrils responsible for the piezoelectricity of bone," ACS Nano, vol. 3, no. 7, pp. 1859–1863, 2009.
[6] E. Fukada and I. Yasuda, "On the piezoelectric effect of bone," J. Phys. Soc. Jpn, vol. 12, no. 10, pp. 1158–1162, 1957.
[7] E. Fukada, H. Ueda, and R. Rinaldi, "Piezoelectric and related properties of hydrated collagen," Biophys. J, vol. 16, no. 8, pp. 911–918, 1976.
[8] K. Ryan *et al,* "Nanoscale piezoelectric properties of self-assembled Fmoc-FF peptide fibrous networks," ACS Appl. Mater. Interfaces, vol. 7, no. 23, pp. 12702–12707, 2015.
[9] A. Kholkin *et al,* "Strong piezoelectricity in bioinspired peptide nanotubes," ACS Nano, vol. 4, no. 2, pp. 610–614, 2010.
[10] S. Guerin, S. A. M. Tofail, and D. Thompson, "Organic piezoelectric materials: milestones and potential," NPG Asia Mater, vol. 11, no. 10, 2019.
[11] D. M Shin; S. W. Hong, and Y. H. Hwang, "Recent advances in organic piezoelectric biomaterials for energy and biomedical applications," Nanomaterials, vol. 10, no.1:123, 2020.
[12] K. Tao *et al*, "Bioinspired stable and photoluminescent assemblies for power generation", Adv. Mater., vol. 31, no.12, pp. 1807481, 2019.
[13] I. W. Park *et al*, "Recent developments and prospects of M13- bacteriophage based piezoelectric energy harvesting devices." Nanomaterials, vol. 10, no. 1: 93, 2020.
[14] J. H. Lee *et al*, "Diphenylalanine peptide nanotube energy harvesters," ACS Nano, vol. 12, no. 8, pp. 8138–8144, 2018.
[15] C. Harnagea *et al,* "Two-dimensional nanoscale structural and functional imaging in individual collagen type I fibrils," Biophys. J, vol. 98, no. 12, pp. 3070–3077, 2010.
[16] M. E. Mycielska and M. B. A. Djamgoz, "Cellular mechanisms of direct-current electric field effects: Galvanotaxis and metastatic disease," J. Cell Sci, vol. 117, no. 9, pp. 1631–1639, 2004.
[17] R. Núñez-Toldrà, F. Vasquez-Sancho, N. Barroca, and G. Catalan, "Investigation of the cellular response to bone fractures: evidence for flexoelectricity," Sci. Rep, vol. 10, no. 1, pp. 1–10, 2020.
[18] D. Denning *et al,* "Electromechanical properties of dried tendon and isoelectrically focused collagen hydrogels," Acta Biomater, vol. 8, no. 8, pp. 3073–3079, 2012.
[19] D. Denning, M. V. Paukshto, S. Habelitz, and B. J. Rodriguez, "Piezoelectric properties of aligned collagen membranes," J. Biomed. Mater. Res. B, vol. 102, no. 2, pp. 284–292, 2014.

[20] F. J. Avila, O. del Barco, and J. M. Bueno, “Polarization dependence of aligned collagen tissues imaged with second harmonic generation microscopy,” J. Biomed. Opt., vol. 20, no. 8, pp. 086001, 2015.
[21] M. Paukshto, G. Fuller, A. Michailov, and S. Remizov, “Optics of sheared liquid-crystal polarizer based on aqueous dispersion of dichroic-dye nano-aggregates,” J. Soc. Inf. Disp, vol. 13, no. 9, pp. 765–772, 2005.
[22] F. Peter *et al*, “Sample-tip interaction of piezoresponse force microscopy in ferroelectric nanostructures,” IEEE Trans. Ultrason. Ferroelectr. Freq. Control, vol. 53, no. 12, pp. 2253–2260, 2006.
[23] S. Morozova and M. Muthukumar, “Electrostatic effects in collagen fibril formation,” J. Chem. Phys, vol. 149, no. 16, pp. 163333, 2018.
[24] V. V. Shvartsman, W. Kleemann, T. Lukasiewicz, and J. Dec, “Nanopolar structure in $Sr_xBa_{1-x}Nb_2O_6$ single crystals tuned by Sr/Ba ratio and investigated by piezoelectric force microscopy,” Phys. Rev. B, vol. 77, no. 5, pp. 054105, 2008.
[25] D. Denning, J. Guyonnet, and B. J. Rodriguez, “Applications of piezoresponse force microscopy in materials research: From inorganic ferroelectrics to biopiezoelectrics and beyond,” Int. Mater. Rev., vol. 61, no. 1, pp. 46–70, 2016.